INTERNATIONAL JOURNAL FOR NUMERICAL METHODS IN FLUIDS
Int. J. Numer. Meth. Fluids 2003; **41**:881–904 (DOI: 10.1002/fld.482)

A new positive-definite regularization of incompressible Navier–Stokes equations discretized with Q1/P0 finite element

Yuzuru Eguchi*,†

Fluid Science Department, Central Research Institute of Electric Power Industry, 1646 Abiko, Abiko-shi, Chiba 270-1194, Japan

SUMMARY

A new regularization method is proposed for the Galerkin approximation of the incompressible Navier–Stokes equations with Q1/P0 element, by newly introducing a square-type linear form into the variational divergence-free constraint regularized with the global pressure jump (GPJ) method. The addition of the square-type linear form is intended to eliminate the hydrostatic pressure mode appearing in confined flows, and to make the discretized matrix positive definite and then non-singular without the pressure pegging trick. Effects of the free parameters for the regularization on the solutions are numerically examined with a 2-D driven cavity flow problem. Furthermore, the convergences in the conjugate gradient iteration for the solution of the pressure Poisson equation are compared among the mixed method, the GPJ method and the present method for both leaky and non-leaky 3-D driven cavity flows. Finally, the non-leaky 3-D cavity flows at different *Re* numbers are solved to compare with the literature data and to demonstrate the accuracy of the proposed method. Copyright © 2003 John Wiley & Sons, Ltd.

KEY WORDS: positive definiteness; regularization; hydrostatic pressure mode; Q1/P0 element; conjugate gradient method; non-leaky driven cavity flow

1. INTRODUCTION

Choice of element type has been one of the most controversial subjects in solving the incompressible viscous fluid flow among the finite element community. Although the Q1/P0 element (combination of multi-linear interpolation for velocity and piecewise-constant for pressure) has been in high favor with the finite element practitioners due to the simple data structure, the element is notorious among the theoreticians because of the violation of the Babuska–Brezzi condition, or so-called 'Inf-Sup condition'. What the theoreticians claim against the Q1/P0 element is true also from a practical viewpoint: that is, Q1/P0 users sometimes encounter very tough problems (e.g. non-leaky driven cavity flow problem) which may not be solved at all, and often suffer from very slow and/or irregular convergence of iterative solvers even for seemingly easy problems.

*Correspondence to: Y. Eguchi, Fluid Science Department, Central Research Institute of Electric Power Industry, 1646 Abiko, Abiko-shi, Chiba, Japan 270-1194.
†E-mail: eguchi@criepi.denken.or.jp

Received 20 March 2002
Revised 6 December 2002

The ill performance of the Q1/P0 solution originates from the rank deficiency of the resulting matrix system and consequent non-uniqueness of the solution (if it exists). To circumvent such difficulty, Hughes and Franca [1] proposed a symmetric finite element formulation for the primitive-variables incompressible Stokes equations by adding the least-square forms of pressure jump (discontinuity) across inter-element boundaries to the classical Galerkin formulation. The formulation was proved to be convergent for any combination of velocity and pressure interpolations [1]. Subsequently, Silvester and Kechkar [2] showed a sufficient condition for the stability (uniqueness up to an arbitrary additive constant) for regularized incompressible Stokes equations, and numerically demonstrated the effectiveness of two possible regularization procedures: the global pressure jump (GPJ) formulation and the local pressure jump formulation. The former one is the same as that proposed by Hughes and Franca [1], while the latter similarly takes account of the pressure jump across inter-element boundaries but only inside each macro-element composed of 2×2 (in 2-D) or $2 \times 2 \times 2$ (in 3-D) Q1/P0 elements. Although the spurious pressure mode can be eliminated with these treatments, the matrix system of a confined flow problem is still singular due to the hydrostatic pressure mode, and the convergence performance of any iterative solvers can be slow and/or irregular. Such ill performance of iterative solution would severely erode the robustness of any sorts of flow analyses ranging from a practical run on a PC to scientific computation on parallel processing systems, since iterative solution of large algebraic system is essential in any such flow analyses.

In the present paper, the author proposes a new regularization for the Q1/P0 approximation of the incompressible Navier–Stokes (NS) equations. In the proposed method, a square-type linear form (a specific bilinear form) is added to the GPJ formulation in order to eliminate the null space of the hydrostatic pressure mode. The resulting matrix system is positive definite and a completely unique solution is obtained without any arbitrary additive constant. The property suggests that the convergence rate of iterative solvers would significantly improve and no trick such as the pressure pegging would be needed any more. The author would like to term the new regularization as the HPMS/GPJ formulation, where HPMS stands for Hydrostatic Pressure Mode Suppression.

The paper is organized as follows: In the following section, the proposed method is explained for the steady incompressible Stokes problem in comparison with the Lagrange multiplier method and the conventional penalty method. In Section 3, finite element implementation with Q1/P0 element as well as the time integration scheme is explained for the solution of the unsteady incompressible NS equations. In Section 4, numerical results are presented to show the effect of the regularization parameters on the accuracy of the solution for the 2-D non-leaky (water-proof) driven cavity flow problem which would be ill-posed in the mixed method. Furthermore, the proposed method is applied to the 3-D cavity flows to demonstrate the accuracy of the solution and the convergence of the conjugate gradient iteration. Finally, some concluding remarks are made in Section 5.

2. REGULARIZATION OF STEADY INCOMPRESSIBLE STOKES EQUATION

Although the actual computation is performed in a segregated manner for velocity and pressure with the unsteady NS equations, the coupled system of the steady incompressible Stokes equation is considered in this section to show the features of the proposed HPMS formulation.

2.1. Weak form

The steady incompressible Stokes equations are written as follows.

$$-\nu u_{i,j,j} + p_{,i} = f_i \quad \text{in } \Omega \tag{1}$$

$$u_{i,j} = 0 \quad \text{in } \Omega \tag{2}$$

where subscripts i and j run from 1 to N_{D}, u_i is the ith velocity component, p is the kinematic pressure (pressure divided by fluid density), f_i is the body force per unit mass, ν is a kinematic viscosity, Ω is the flow domain in space dimension N_{D} ($=2$ or 3) and $()_{,j}$ denotes the spatial derivative in the jth direction. Summation convention is used for the repeated subscripts. Only the Dirichlet-type non-homogeneous boundary condition (BC) is assumed here to supplement Equations (1) and (2).

$$u_i = b_i \quad \text{on } \Gamma_{\mathrm{all}} \tag{3}$$

where Γ_{all} denotes the whole boundary of Ω and the prescribed velocity b_i is assumed to satisfy the following solvability condition:

$$\int_{\Gamma_{\mathrm{all}}} b_i n_i \, \mathrm{d}\Gamma = 0 \tag{4}$$

where n_i is the unit normal vector outwardly standing on the boundary Γ_{all}.

The weak forms of Equations (1) and (2) can be set up using arbitrary weighting functions w_k and q, belonging to the function spaces V_0 and P, respectively, which are defined below:

$$V_{\alpha_k} = \left\{ w_k \,\middle|\, \int_\Omega w_k^2 \, \mathrm{d}\Omega < \infty, \int_\Omega w_{k,j}^2 \, \mathrm{d}\Omega < \infty, w_k = \alpha_k \quad \text{on } \Gamma_{\mathrm{all}} \ (j,k = 1, \ldots, N_{\mathrm{D}}) \right\} \tag{5}$$

$$P = \left\{ q \,\middle|\, \int_\Omega q^2 \, \mathrm{d}\Omega < \infty \right\} \tag{6}$$

The discretized version of the weak forms are written as follows by introducing finite-dimensional subspaces $V_{b_i}^h \subset V_{b_i}$ and $P^h \subset P$.

Weak form: Find $u_i^h \in V_{b_i}^h$ and $p^h \in P^h$, such that

$$\nu \int_\Omega u_{i,j}^h w_{k,j}^h \, \mathrm{d}\Omega - \int_\Omega p^h w_{k,i}^h \, \mathrm{d}\Omega = \int_\Omega f_i w_k^h \, \mathrm{d}\Omega \quad \forall w_k^h \in V_0^h \tag{7}$$

$$\int_\Omega q^h u_{i,i}^h \, \mathrm{d}\Omega = 0 \quad \forall q^h \in P^h \tag{8}$$

The matrix analogue of the above weak form problem is expressed by

$$\begin{pmatrix} \nu\mathbf{K} & -\mathbf{C} \\ \mathbf{C}^{\mathrm{T}} & \mathbf{0} \end{pmatrix} \begin{Bmatrix} \mathbf{U} \\ \mathbf{P} \end{Bmatrix} = \begin{Bmatrix} \mathbf{F} \\ \mathbf{B} \end{Bmatrix} \tag{9}$$

where $\mathbf{K}$ is the diffusion matrix (symmetric positive definite), $\mathbf{C}$ is the gradient matrix, $\mathbf{C}^{\mathrm{T}}$ is the divergence matrix, $\mathbf{F}$ is the body force vector, $\mathbf{B}$ is a vector resulted from the imposition of velocity BC on Γ_{all}, $\mathbf{U}$ is a vector composed of unknown velocity components and $\mathbf{P}$ is a vector composed of unknown pressures. Gresho and Sani [3] show that any and all null vectors of the matrix in Equation (9) are pure pressure modes $\{\mathbf{0}^{\mathrm{T}}\mathbf{P}_m^{i\mathrm{T}}\}^{\mathrm{T}}$ where $\mathbf{C}\mathbf{P}_m^i = \mathbf{0}$ and $\mathbf{P}_m^i \neq \mathbf{0}$, and that the solution exists if and only if the following condition is satisfied.

$$\mathbf{P}_m^{i\mathrm{T}}\mathbf{B} = \mathbf{0} \quad (i = 1, \ldots, N_{\mathrm{null}}\text{: number of null vectors of } \mathbf{C}) \tag{10}$$

If the approximation spaces $V_{b_i}^h$ and P^h are spanned by the multi-linear interpolation functions and the piecewise constant functions, respectively, on Q1/P0 finite elements, then the mixed approximation fails the Babuska–Brezzi test and the uniqueness of the solution $\{\mathbf{U}^{\mathrm{T}}\ \mathbf{P}^{\mathrm{T}}\}^{\mathrm{T}}$ up to an arbitrary additive constant is not guaranteed for the matrix system (9). When the solution is not unique, there should be at least one null vector $\mathbf{P}_m^i$ (spurious pressure mode) other than the physical one (hydrostatic pressure mode) whose components are equal to each other.

2.2. A new regularization method: HPMS/GPJ formulation

To escape from the Babuska–Brezzi test and to manage to achieve the complete uniqueness of the Q1/P0 solutions in another way, the present author newly proposes the following regularization for Equation (8).

$$\int_\Omega q^h u_{i,i}^h \, \mathrm{d}\Omega + J(q^h, p^h) + H(q^h)H(p^h) = 0 \quad \forall q^h \in P^h \tag{11}$$

The definitions of the added bilinear forms are given by

$$J(q^h, p^h) = \frac{\beta\tau}{L_J^2} \sum_{i=1}^{i=N_s} h_i \int_{\Gamma_i} [q^h][p^h] \, \mathrm{d}\Gamma \tag{12}$$

$$H(q^h)H(p^h) = \frac{\lambda\tau}{L_H^5} \int_\Omega q^h \, \mathrm{d}\Omega \int_\Omega p^h \, \mathrm{d}\Omega \tag{13}$$

where β and λ are non-dimensional positive parameters, while τ and L_J (L_H) are a global time scale and global length scales for Equation (11) to be dimensionally consistent. In Equation (12), N_s is the number of interior inter-element edges in 2-D or faces in 3-D, and h_i denotes a representative mesh length for an interface Γ_i, e.g. the element edge length in 2-D or the element face diameter in 3-D. The parenthesis [ ] denotes the jump operator which measures the difference of the argument across an inter-element edge or face.

The GPJ term, $J(q^h, p^h)$ was originally introduced by Hughes and Franca [1] and subsequently examined with numerical tests by Silvester and Kechkar [2]. The GPJ term is supposed to suppress the spurious pressure mode (checkerboard-type pressure oscillation). On the other hand, the product of two linear forms, $H(q^h)H(p^h)$, is newly introduced in the present paper to suppress the hydrostatic pressure mode. The idea comes from the penalty formulation where the constraint, $H(p^h) = 0$, is incorporated into a variational setting as a penalty term. Let us call the addition of the square-type linear form, $H(q^h)H(p^h)$, as the Hydrostatic Pressure Mode Suppression (HPMS) formulation.

Annihilation of the hydrostatic pressure mode can be seen by taking $q^h = 1$ in the whole domain Ω in Equation (11). The equation gives rise to the following, considering $[q^h] = 0$ on every inter-element face.

$$\int_\Omega u^h_{i,i}\,\mathrm{d}\Omega + \lambda' \int_\Omega p^h\,\mathrm{d}\Omega = 0 \tag{14}$$

where λ' is used for $\lambda\tau\Omega/L_H^5$ with the domain volume $\Omega = \int_\Omega \mathrm{d}\Omega$. Applying the divergence theorem to the first term and considering the solvability condition (4) lead to the following pressure constraint (or annihilation of the hydrostatic pressure mode):

$$\int_\Omega p^h\,\mathrm{d}\Omega = 0 \tag{15}$$

On the other hand, taking $q^h = 1$ in a specific element domain, Ω_e, only and $q^h = 0$ elsewhere in Equation (11) gives rise to the following, considering Equation (15) and $[q^h] = 0$ on every inter-element face except around the element e where $[q^h] = 1$:

$$\int_{\Omega_\mathrm{e}} u^h_{i,i}\,\mathrm{d}\Omega + \frac{\beta\tau}{L_J^2} \sum_{i=1}^{i=N_s^e} h_i(p_e^h - p^h_{e(i)})\Gamma_i = 0 \tag{16}$$

where $(p_e^h - p^h_{e(i)})$ denotes the pressure jump across element e and its neighbouring element $e(i)$. N_s^e denotes the number of faces through which element e contacts the neighbouring elements, while Γ_i denotes the area. Equation (16) suggests that the element-level velocity divergence would be sensitive to β but independent of parameter λ. The insensitiveness of the solution to the parameter λ is very preferable in carrying out actual computations in marked contrast with the conventional penalty method as explained in Section 2.4.

2.3. Comparison with the Lagrange multiplier method

The hydrostatic pressure constraint, $\int_\Omega p^h\,\mathrm{d}\Omega = 0$, or $H(p^h) = 0$, can be dealt with the Lagrange multiplier method besides the present method. To incorporate the hydrostatic pressure constraint with the Lagrange multiplier method, the following functional is introduced.

$$L(\mathbf{V}, \mathbf{X}, \omega) = \mathbf{V}^\mathrm{T}\left(\frac{1}{2}\nu\mathbf{K}\mathbf{V} - \mathbf{F}\right) + \mathbf{X}^\mathrm{T}(\mathbf{B} - \mathbf{C}^\mathrm{T}\mathbf{V}) - \omega\mathbf{R}^\mathrm{T}\mathbf{X} \tag{17}$$

where $\mathbf{V}$ is the vector of discretized velocities, $\mathbf{X}$ is the vector of discretized pressures (or Lagrange multipliers for the incompressibility constraint), and ω is the Lagrange multiplier for the constraint of $\mathbf{R}^\mathrm{T}\mathbf{X} = 0$. Vector $\mathbf{R}$ is defined by

$$\mathbf{R} = \{\Omega_1, \Omega_2, \ldots, \Omega_{N_e}\}^\mathrm{T} \tag{18}$$

to form the pressure integral, $\mathbf{R}^\mathrm{T}\mathbf{P} = \int_\Omega p^h\,\mathrm{d}\Omega$, where Ω_k is the volume of kth element, and N_e is the number of total elements. The first variation of functional (17), δL, is given as

$$\begin{aligned}\delta L(\mathbf{V}, \mathbf{X}, \omega) = {} & \delta\mathbf{V}^\mathrm{T}(\nu\mathbf{K}\mathbf{V} - \mathbf{C}\mathbf{X} - \mathbf{F}) \\ & + \delta\mathbf{X}^\mathrm{T}(\mathbf{B} - \mathbf{C}^\mathrm{T}\mathbf{V} - \omega\mathbf{R}) \\ & - \delta\omega\mathbf{R}^\mathrm{T}\mathbf{X}\end{aligned} \tag{19}$$

The extremum point of functional (17) is derived by setting the first variation δL at zero, satisfying the following matrix equation:

$$\begin{pmatrix} \nu\mathbf{K} & -\mathbf{C} & \mathbf{0} \\ \mathbf{C}^{\mathrm{T}} & \mathbf{0} & \mathbf{R} \\ \mathbf{0} & -\mathbf{R}^{\mathrm{T}} & \mathbf{0} \end{pmatrix} \begin{Bmatrix} \mathbf{V} \\ \mathbf{X} \\ \omega \end{Bmatrix} = \begin{Bmatrix} \mathbf{F} \\ \mathbf{B} \\ 0 \end{Bmatrix} \tag{20}$$

The matrix of Equation (20) is not positive definite because of the zero entries at the diagonal positions. Therefore, the convergence of the conjugate gradient (CG) method is not guaranteed for the iterative solution of Equation (20).

On the other hand, Equations (7) and (11) derived from the proposed HPMS/GPJ formulation are summarized in the following matrix form:

$$\begin{pmatrix} \nu\mathbf{K} & -\mathbf{C} \\ \mathbf{C}^{\mathrm{T}} & \beta\mathbf{J} + \lambda\mathbf{H} \end{pmatrix} \begin{Bmatrix} \mathbf{U} \\ \mathbf{P} \end{Bmatrix} = \begin{Bmatrix} \mathbf{F} \\ \mathbf{B} \end{Bmatrix} \tag{21}$$

where matrices $\mathbf{J}$ and $\mathbf{H}$ originate from Equations (12) and (13), respectively. The positive definiteness of the above matrix can be easily proven, which mathematically implies the existence and the uniqueness of the solution and guarantees the convergence of the CG iteration. It should be noted that the matrix $\mathbf{H}$ is a full matrix, and that the work of matrix-by-vector multiplication needed in each CG step is apparently proportional to the square of the number of degree-of-freedom of pressures. Although such a straightforward matrix-by-vector multiplication is prohibitively expensive, the operation can be reduced to linearly proportional work, because the matrix is expressed in the following form:

$$\mathbf{H} = (\tau/L_{\mathrm{H}}^5)\mathbf{R}\mathbf{R}^{\mathrm{T}} \tag{22}$$

Then, once the inner product $a = \mathbf{R}^{\mathrm{T}}\mathbf{P}$ is computed, the matrix-by-vector multiplication is easily computed as the scalar-by-vector multiplication, such as

$$\mathbf{H}\mathbf{P} = (a\tau/L_{\mathrm{H}}^5)\mathbf{R} \tag{23}$$

2.4. Comparison with the conventional penalty method

Since the present HPMS formulation is considered as a sort of a penalty method (only for the hydrostatic pressure constraint, but not for the incompressibility constraint), let us compare with the conventional penalty method. The conventional or standard penalty method (hereafter, the penalty method) was originally introduced by Hughes *et al.* [4] in context of the finite element solutions of the incompressible NS equations, to approximately satisfy the incompressibility constraint. As the by-product, the penalty solutions also satisfy the hydrostatic pressure constraint and the matrix system of the penalty method is positive definite, as shown below.

The incompressibility constraint, Equation (8), is regularized in the penalty method as follows:

$$\int_{\Omega} q^h u_{i,i}^h \, \mathrm{d}\Omega + I(q^h, p^h) = 0 \quad \forall q^h \in P^h \tag{24}$$

where the bilinear form $I(q^h, p^h)$ is defined as follows:

$$I(q^h, p^h) = \frac{\varepsilon\tau}{L_I^2} \int_\Omega q^h p^h \, \mathrm{d}\Omega \tag{25}$$

In the above, ε is a non-dimensional penalty parameter and L_I is a global length scale for dimensional adjustment. The resulting matrix system of the incompressible Stokes flow via the penalty method is expressed as follows:

$$\begin{pmatrix} \nu\mathbf{K} & -\mathbf{C} \\ \mathbf{C}^{\mathrm{T}} & \varepsilon\mathbf{Q} \end{pmatrix} \begin{Bmatrix} \mathbf{U} \\ \mathbf{P} \end{Bmatrix} = \begin{Bmatrix} \mathbf{F} \\ \mathbf{B} \end{Bmatrix} \tag{26}$$

where $\mathbf{Q}$ is a matrix resulting from $I(q^h, p^h)$ in Equation (25) and is a diagonal matrix in using the Q1/P0 element. The positive definiteness of the matrix of Equation (26) can be easily confirmed by the positive definiteness of $\mathbf{K}$ and $\mathbf{Q}$, meaning that the penalty solution is completely unique. The annihilation of the hydrostatic pressure mode can also be confirmed by taking $q^h = 1$ in the whole domain Ω in Equation (24) as follows.

$$\int_\Omega u^h_{i,i} \, \mathrm{d}\Omega + \varepsilon' \int_\Omega p^h \, \mathrm{d}\Omega = 0 \tag{27}$$

where ε' is used for $\varepsilon\tau/L_{\mathrm{I}}^2$. Applying the Gauss divergence theorem to the first term and considering the solvability condition (4) lead to $\int_\Omega p^h \, \mathrm{d}\Omega = 0$.

The main drawback of the penalty method is the sensitivity of solution to the penalty parameter ε (in contrast with insensitivity of the HPMS solution to the parameter λ). The sensitivity can be shown by the following equation which is obtained by taking $q^h = 1$ in an element domain Ω_{e} and $q^h = 0$ elsewhere in Equation (24):

$$\int_{\Omega_{\mathrm{e}}} u^h_{i,i} \, \mathrm{d}\Omega + \varepsilon' \int_{\Omega_{\mathrm{e}}} p^h \, \mathrm{d}\Omega = 0 \tag{28}$$

Equation (28) suggests that the element-level divergence-free condition would deteriorate for a large ε value, because each element pressure integral $\int_{\Omega_{\mathrm{e}}} p^h \, \mathrm{d}\Omega$ is not always zero in general if the penalty pressure is accurate enough. Besides, when ε is small, the matrix in Equation (26) approaches that of the original mixed method and becomes ill-conditioned, precluding the use of iterative solvers. Then, the penalty method is useless in practice.

Gresho and Sani [3] and Sani *et al.* [5] showed the behaviour of the penalty solutions under well-posed and ill-posed conditions, as follows. The penalty pressure $\mathbf{P}$ is $\mathbf{Q}$-orthogonal to the pressure mode $\mathbf{P}^i_m$ of the mixed method (i.e. $\mathbf{P}^{i\mathrm{T}}_m \mathbf{Q}\mathbf{P} = 0$), if the mixed approximation problem is well-posed (i.e. $\mathbf{P}^{i\mathrm{T}}_m \mathbf{B} = \mathbf{0}$). This implies that the penalty pressure $\mathbf{P}$ would be free from both the spurious and physical pressure modes $\mathbf{P}^i_m$ for such 'well-posed' problems. On the other hand, if the mixed problem is ill-posed (i.e. $\mathbf{P}^{i\mathrm{T}}_m \mathbf{B} \neq 0$), the penalty pressure will be very large $\boldsymbol{O}(\varepsilon^{-1})$ due to the relation of $\mathbf{P}^{i\mathrm{T}}_m \mathbf{Q}\mathbf{P} = \varepsilon^{-1} \mathbf{P}^{i\mathrm{T}}_m \mathbf{B}$ and the associated velocities are not physical. Therefore, the penalty method is not applicable to such 'ill-posed' problems, even though the solution uniquely exists.

Similar discussion is applicable to the present HPMS/GPJ formulation, by pre-multiplying Equation (21) by the null vector of the mixed method $\{\mathbf{0}^{\mathrm{T}} \ \mathbf{P}^{i\mathrm{T}}_m\}$.

$$\mathbf{P}^{i\mathrm{T}}_m (\beta\mathbf{J} + \lambda\mathbf{H})\mathbf{P} = \mathbf{P}^{i\mathrm{T}}_m \mathbf{B} \quad (i = 1, \ldots, N_{\mathrm{null}}) \tag{29}$$

Equation (29) implies that, if the problem is ill-posed in the mixed method (i.e. $\mathbf{P}_m^{i\mathrm{T}}\mathbf{B} \neq 0$), then $\mathbf{P}_m^{i\mathrm{T}}(\beta\mathbf{J} + \lambda\mathbf{H})\mathbf{P} \neq 0$. Since the parameter λ can be much larger theoretically than the penalty parameter ε due to the λ-insensitiveness shown in Section 2.2, it is expected that the HPMS/GPJ solution will be acceptable even for the 'ill-posed' problems. To confirm such expectation, numerical tests are conducted for one of the 'ill-posed' problems, i.e. a non-leaky 2-D cavity flow problem in Section 4 to see the performance of the HPMS/GPJ solutions under such a tough condition.

3. FINITE ELEMENT IMPLEMENTATION

3.1. Basic equations

The following 3-D incompressible transient NS equations are used as the basic equations for the finite element formulation:

$$\dot{u}_i + u_j u_{i,j} + p_{,i} - \nu u_{i,j,j} = f_i \quad \text{in } \Omega \tag{30}$$

$$u_{i,i} = 0 \quad \text{in } \Omega \tag{2}$$

where the superposed dot denotes the time derivative and subscripts i and j run from 1 to 3. The following three types of time-independent BCs are assumed to supplement Equations (30) and (2):

$$u_i = u_i^{\mathrm{BC}}(x_1, x_2, x_3) \qquad \text{on } \Gamma_{\mathrm{u}} \tag{31}$$

$$\chi_i = \chi_i^{\mathrm{BC}}(x_1, x_2, x_3) \qquad \text{on } \Gamma_{\chi} \tag{32}$$

$$u_i n_i = 0, \quad \chi_i t_i^1 = \chi_i t_i^2 = 0 \quad \text{on } \Gamma_{\mathrm{s}} \tag{33}$$

where n_i, t_i^1 and t_i^2 are the unit normal vector and two unit tangential vectors on smooth surface Γ_{s} and they are assumed to satisfy

$$n_i t_i^1 = n_i t_i^2 = t_i^1 t_i^2 = 0 \quad \text{on } \Gamma_{\mathrm{s}} \tag{34}$$

The traction divided by fluid density, χ_i, is defined as follows:

$$\chi_i = (-p\delta_{ij} + \nu u_{i,j}) n_j \tag{35}$$

In the above, Γ_{u} denotes the velocity-prescribed boundary; Γ_{χ} denotes the traction-prescribed boundary; Γ_{s} denotes the slip wall or symmetry plane and δ_{ij} is the Kronecker delta. Although it is assumed that the whole boundary of the computational domain is covered with the three types of boundary conditions without overlapping each other, a special focus is placed in this paper on the following case where the hydrostatic pressure mode would appear in conventional methods.

$$\Gamma_{\mathrm{u}} \cup \Gamma_{\mathrm{s}} = \Gamma_{\mathrm{all}} \text{ (whole boundary)}, \quad \Gamma_{\chi} = \phi \text{ (null)} \tag{36}$$

3.2. Spatial discretization and time integration

Using Q1/P0 element, the momentum equation (30) is spatially discretized with the conventional Galerkin finite element method, while the continuity equation (2) is regularized and spatially discretized with the proposed HPMS/GPJ formulation. The final ordinary differential equations are summarized in the following form:

$$\mathbf{M}\dot{\mathbf{U}} + \mathbf{A}\mathbf{U} + \nu\mathbf{K}\mathbf{U} - \mathbf{C}\mathbf{P} = \mathbf{F} + \mathbf{F}_{\mathrm{t}} \tag{37}$$

$$\mathbf{C}^{\mathrm{T}}\mathbf{U} + \beta\mathbf{J}\mathbf{P} + \lambda\mathbf{H}\mathbf{P} = \mathbf{0} \tag{38}$$

where $\mathbf{M}$ is the consistent mass matrix, $\mathbf{A}$ is the convection matrix and $\mathbf{F}_{\mathrm{t}}$ is the traction vector. Hereafter, $\mathbf{U}$ denotes a velocity vector composed of all nodal velocities, both specified and unspecified, and the velocity BCs are introduced during the time integration process by pre-multiplying the acceleration increment, $\Delta\mathbf{a}$, by the BC imposition matrix, $\mathbf{G}$, which is composed of the following 3×3 sub-matrices g_{ij}^{α} corresponding to each nodal velocity, $U_{j\alpha}$ at node number α.

$$g_{ij}^{\alpha} = \begin{cases} 0 & \text{for velocity-prescribed nodes on } \Gamma_{\mathrm{u}} \\ \delta_{ij} - n_{i\alpha}n_{j\alpha} & \text{for slip-wall nodes on } \Gamma_{\mathrm{s}} \\ \delta_{ij} & \text{otherwise (for internal nodes and traction-prescribed nodes)} \end{cases} \tag{39}$$

where $n_{i\alpha}$ denotes the unit normal vector at the slip-wall node. The BC imposition matrix guarantees the new velocity updated by acceleration increment $\Delta a_{j\alpha}$ multiplied by a controlled time increment $\gamma\,\Delta t$, $(U_{i\alpha} + \gamma\,\Delta t g_{ij}^{\alpha}\,\Delta a_{j\alpha})$, to satisfy the velocity BCs, as far as the old velocity $U_{i\alpha}$ does. More detailed explanation of the BC imposition is given in Reference [6].

Starting with an initial velocity $\mathbf{U}_0$, satisfying the velocity BCs, and an initial pressure, $\mathbf{P}_0$, the time integration of Equations (37) and (38) is performed in a segregated manner with the predictor/multi-corrector (PMC) scheme [7] as summarized in Table I. The PMC scheme is fully explicit time-marching algorithm, although only the regularized divergence-free constraint and the associated pressure are treated implicitly. The lumped mass matrix is thoroughly used to avoid the full inversion of the consistent mass matrix, except for the mass matrix multiplication appearing in Step 1 in the multi-corrector phase as seen in Table I. The participation of the consistent mass matrix helps to reduce numerical errors inherent in fully explicit methods with the mass lumping [7, 8].

3.3. Pressure poisson equation

The unique Poisson equation appearing in Step 4 in the multi-corrector phase is formed by the requirement of the velocity BC imposition for unknown acceleration increment, $\Delta\mathbf{a}^k$, and the requirement of the regularized velocity-divergence condition for the unknown velocity and pressure at $(k+1)$th multi-corrector iteration step, $\mathbf{U}^{k+1}$ and $\mathbf{P}^{k+1}$. That is

$$\Delta\mathbf{a}^k = \Delta\mathbf{a}^{*k} + \mathbf{G}\underline{\mathbf{M}}^{-1}\mathbf{C}\Delta\mathbf{P}^k \tag{40}$$

$$\mathbf{C}^{\mathrm{T}}\mathbf{U}^{k+1} + \beta\mathbf{J}\mathbf{P}^{k+1} + \lambda\mathbf{H}\mathbf{P}^{k+1} = 0$$

$$\text{or} \quad \mathbf{C}^{\mathrm{T}}(\mathbf{U}^k + \gamma\,\Delta t\,\Delta\mathbf{a}^k) + \beta\mathbf{J}(\mathbf{P}^k + \Delta\mathbf{P}^k) + \lambda\mathbf{H}(\mathbf{P}^k + \Delta\mathbf{P}^k) = 0 \tag{41}$$

Table I. Algorithm of the predictor/multi-corrector time integration with the HPMS/GPJ formulation.

[O] Initialization phase		
1	Initialize time and time step counter	$t=0,\ n=0$
2	Set initial velocity and pressure	$\mathbf{U}(n)=\mathbf{U}_0,\ \mathbf{P}(n)=\mathbf{P}_0$
3	Compute the initial acceleration	$\mathbf{a}(n)=\underline{\mathbf{M}}^{-1}(\mathbf{F}+\mathbf{F}_t-\mathbf{A}\mathbf{U}_0-\nu\mathbf{K}\mathbf{U}_0+\mathbf{C}\mathbf{P}_0)$
4	Impose the velocity BC	$\mathbf{a}(n)=\mathbf{G}\mathbf{a}(n)$
[I] Predictor phase		
1	Reset inner-iteration counter	$k=0$
2	Set initial values of velocity, acceleration	$\mathbf{U}^k=\mathbf{U}(n)+\Delta t(1-\gamma)\mathbf{a}(n),\quad \mathbf{a}^k=0,$
	and pressure for next step, $n+1$	$\mathbf{P}^k=\mathbf{P}(n)$
[II] Multi-corrector phase		
1	Compute intermediate acceleration increment	$\Delta\mathbf{a}^{*k}=\underline{\mathbf{M}}^{-1}(\mathbf{F}+\mathbf{F}_t-\mathbf{M}\mathbf{a}^k-\nu\mathbf{K}\mathbf{U}^k-\mathbf{A}\mathbf{U}^k+\mathbf{C}\mathbf{P}^k)$
2	Impose velocity BC	$\Delta\mathbf{a}^{*k}=\mathbf{G}\,\Delta\mathbf{a}^{*k}$
3	Compute intermediate velocity	$\mathbf{U}^{*k}=\mathbf{U}^k+\gamma\,\Delta t\,\Delta\mathbf{a}^{*k}$
4	Solve pressure Poisson equation	$\mathbf{C}^{\mathrm{T}}\mathbf{G}\underline{\mathbf{M}}^{-1}\mathbf{C}\Delta\mathbf{P}^k+\frac{\beta}{\gamma\Delta t}\mathbf{J}\Delta\mathbf{P}^k+\frac{\lambda}{\gamma\Delta t}\mathbf{H}\Delta\mathbf{P}^k$
	to yield pressure increment $\Delta\mathbf{P}^k$	$=-\frac{1}{\gamma\Delta t}\mathbf{C}^{\mathrm{T}}\mathbf{U}^{*k}-\frac{\beta}{\gamma\Delta t}\mathbf{J}\mathbf{P}^k-\frac{\lambda}{\gamma\Delta t}\mathbf{H}\mathbf{P}^k$
5	Correct acceleration increment	$\Delta\mathbf{a}^k=\Delta\mathbf{a}^{*k}+\mathbf{G}\underline{\mathbf{M}}^{-1}\mathbf{C}\Delta\mathbf{P}^k$
6	Correct velocity	$\mathbf{U}^{k+1}=\mathbf{U}^k+\gamma\,\Delta t\,\Delta\mathbf{a}^k$
7	Correct acceleration	$\mathbf{a}^{k+1}=\mathbf{a}^k+\Delta\mathbf{a}^k,$
8	Correct pressure	$\mathbf{P}^{k+1}=\mathbf{P}^k+\Delta\mathbf{P}^k,$
9	IF $(k+1)<K_{\max}$,	Then: bump inner iteration step, $k=k+1$, and iterate [II]
		Else: advance time integration $t=t+\Delta t,$
		$\mathbf{U}(n+1)=\mathbf{U}^{k+1},\ \mathbf{a}(n+1)=\mathbf{a}^{k+1},\ \mathbf{P}(n+1)=\mathbf{P}^{k+1},$
		$n=n+1$, and return to [I]

* $\underline{\mathbf{M}}$: lumped mass matrix; $\mathbf{M}$: consistent mass matrix; Δt: time increment; γ: time integration parameter; $K_{\max}$: upper limit of the multi-corrector iteration.

where matrix $\underline{\mathbf{M}}$ is the lumped mass matrix and vectors $\mathbf{P}^k$, $\Delta\mathbf{P}^k$ and $\Delta\mathbf{a}^{*k}$ are known pressure, unknown pressure increment and known acceleration increment, while Δt and γ are the time increment and the time integration parameter. Elimination of $\Delta\mathbf{a}^k$ from the above leads to the following Poisson equation:

$$\mathbf{C}^{\mathrm{T}}\mathbf{G}\underline{\mathbf{M}}^{-1}\mathbf{C}\Delta\mathbf{P}^k+\frac{\beta}{\gamma\Delta t}\mathbf{J}\Delta\mathbf{P}^k+\frac{\lambda}{\gamma\Delta t}\mathbf{H}\Delta\mathbf{P}^k=-\frac{1}{\gamma\Delta t}\mathbf{C}^{\mathrm{T}}\mathbf{U}^{*k}-\frac{\beta}{\gamma\Delta t}\mathbf{J}\mathbf{P}^k-\frac{\lambda}{\gamma\Delta t}\mathbf{H}\mathbf{P}^k \tag{42}$$

where $\mathbf{U}^{*k} = \mathbf{U}^k + \gamma \Delta t \, \Delta \mathbf{a}^{*k}$ is employed. The matrix of the Poisson equation (42) is positive definite and symmetric, which is solved by the preconditioned conjugate gradient (PCG) method.

4. NUMERICAL RESULTS

In the following computation, all computations are performed with a 3-D analysis code. The pseudo 2-D computations in Section 4.1 are done with a 3-D slab model where a 2-D mesh is expanded in the thickness direction with single element layer. The following values are used for the global quantities appearing in Equations (12) and (13):

$$\tau = \gamma \Delta t$$

$$L_j^2 = S/N_e \text{ in 2-D slab problems, } (\Omega/N_e)^{2/3} \text{ in 3-D problems}$$

$$h_i = \text{square root of inter-element face area of } \Gamma_i$$

$$L_H^5 = \Omega L_J^2$$

where $S(=\Omega/d)$ is the whole 2-D computational area of the slab with thickness d, Ω is the whole computational volume, and N_e is number of total elements. In the time integration, $\Delta t = 0.001$, $\gamma = 0.6$ and $K_{\max} = 2$ (two-pass scheme) are employed thoroughly. The diagonal scaling is used as the preconditioner of the PCG method and the PCG iteration is fixed at 100 steps except the convergence tests in Section 4.2.

4.1. Two-dimensional non-leaky driven cavity flow

The 2-D driven cavity flow problem is solved using a 3-D slab model of $50 \times 50 \times 1$ Q1/P0 finite elements. The upper lid, except the corner nodes, is driven at unit velocity, while the three side walls, including all the corners, are assumed as the non-slip boundaries (i.e. 'non-leaky' cavity). The rest of the two boundaries on 2-D flow areas are symmetry planes where the slip-wall conditions are imposed. The problem is ill-posed in the Q1/P0 mixed method if the number of the elements across the driven lid is even (e.g. Reference [3]). The present mesh division is the case and the computation should be tough or impossible with the Q1/P0

Table II. Effect of parameter β on quasi-steady velocity solutions and L_2 norm of velocity-divergence.

β	λ	u-velocity*	v-velocity* ($\times 10^{-2}$)	$(\int_S \lvert u_{i,i}^h \rvert^2 \, \mathrm{d}S)^{1/2}$
0.01		−0.21106	5.7473	0.07691
0.1		−0.20988	5.7335	0.1578
1	1×10^{-6}	−0.20880	5.6097	0.3905
10		−0.19928	4.5455	0.7823
100		−0.15185	0.29215	1.229
Ghia *et al.* [9]		−0.20581	5.454	N.A.

* Velocity solutions at the cavity centre node.

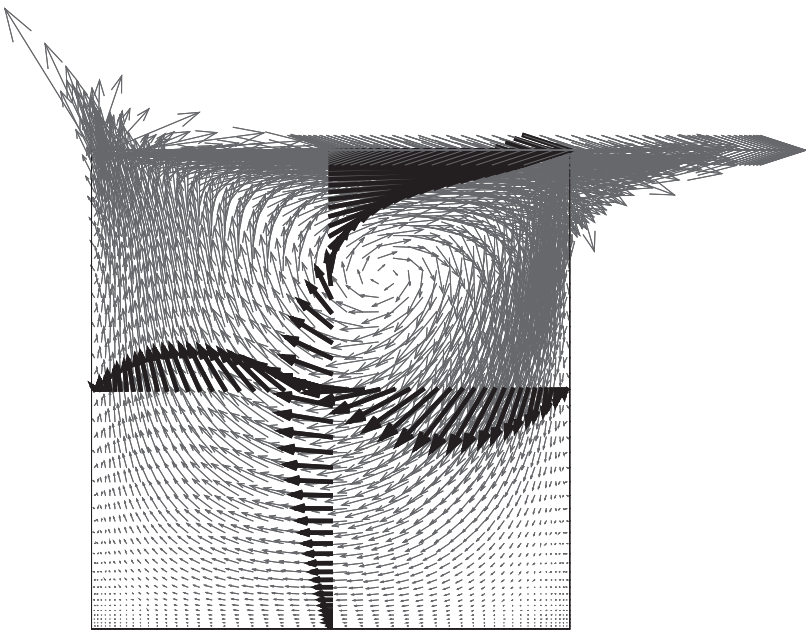

(a)

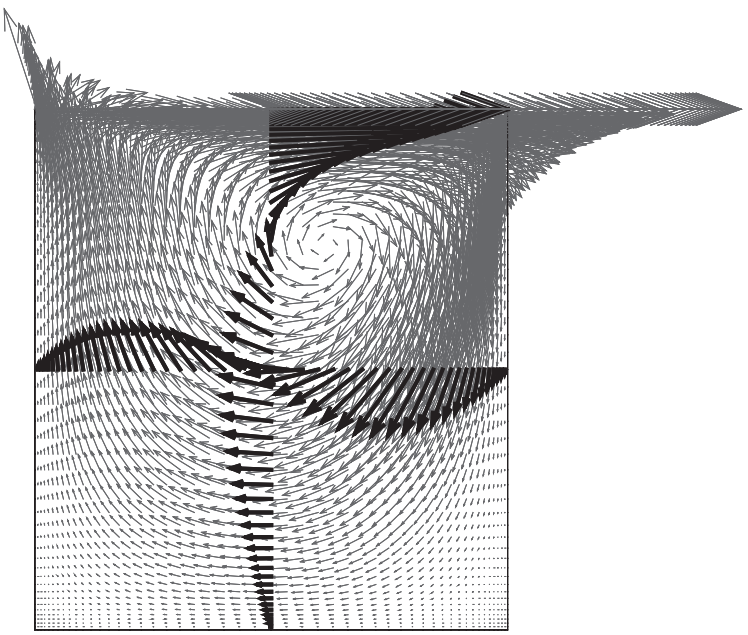

(b)

Figure 1. Velocity vectors: (a) $\beta = 0.01$, $\lambda = 1 \times 10^{-6}$; (b) $\beta = 1$, $\lambda = 1 \times 10^{-6}$ and (c) $\beta = 100$, $\lambda = 1 \times 10^{-6}$.

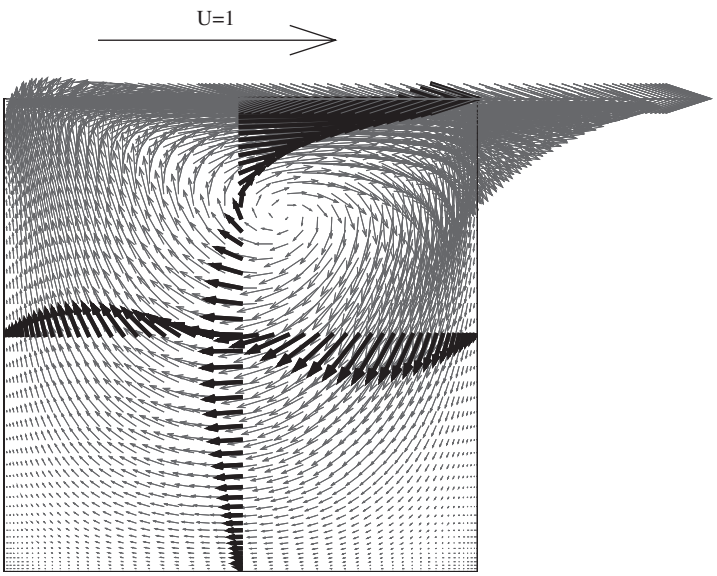

(c)

Figure 1. *Continued.*

element. In this section, sensitivity of the regularization parameters, β and λ, is numerically examined with this tough problem before the real 3-D computation. The kinematic viscosity of fluid, v, is set at 0.01, then the Re number at 100 based on the unit cavity width or depth.

4.1.1. β-sensitivity. The quasi-steady state solutions are obtained with various values of β ranging from 0.01 to 100. Table II shows the results of the computed nodal velocity at the cavity centre in comparison with the solution given by Ghia *et al.* [9]. The table also includes the L_2-norm of divergence of velocity over the 2-D flow area, which is defined as $(\int_S |u^h_{i,i}|^2 \, \mathrm{d}S)^{1/2}$. The results show that the velocity tends to divert from the divergence-free condition as the parameter β increases, and that the difference from the Ghia's solution seems to be minimum around $\beta = 1$. Figures 1(a)–1(c) illustrate the velocity vectors for the typical cases in Table II, while Figures 2(a)–2(c) show the corresponding element pressures without any filtering. It is seen in these figures that the velocity vectors become less oscillatory and the spurious pressure mode tends to fade out, as the parameter β increases. The element-level divergences of velocity are also computed and illustrated in Figures 3(a)–3(c) without any filtering. These figures imply that the incompressibility constraint severely deteriorates for $\beta = 100$, while the condition is almost satisfied everywhere except around the upper two corners for $\beta = 1$. These numerical tests suggest that $\beta = 1$ is a good choice, although the solutions are rather sensitive to the parameter β as demonstrated by Silvester and Kechkar [2] who proposed a less sensitive scheme, i.e. the local pressure jump formulation with the $2 \times 2(\times 2)$ macroelement.

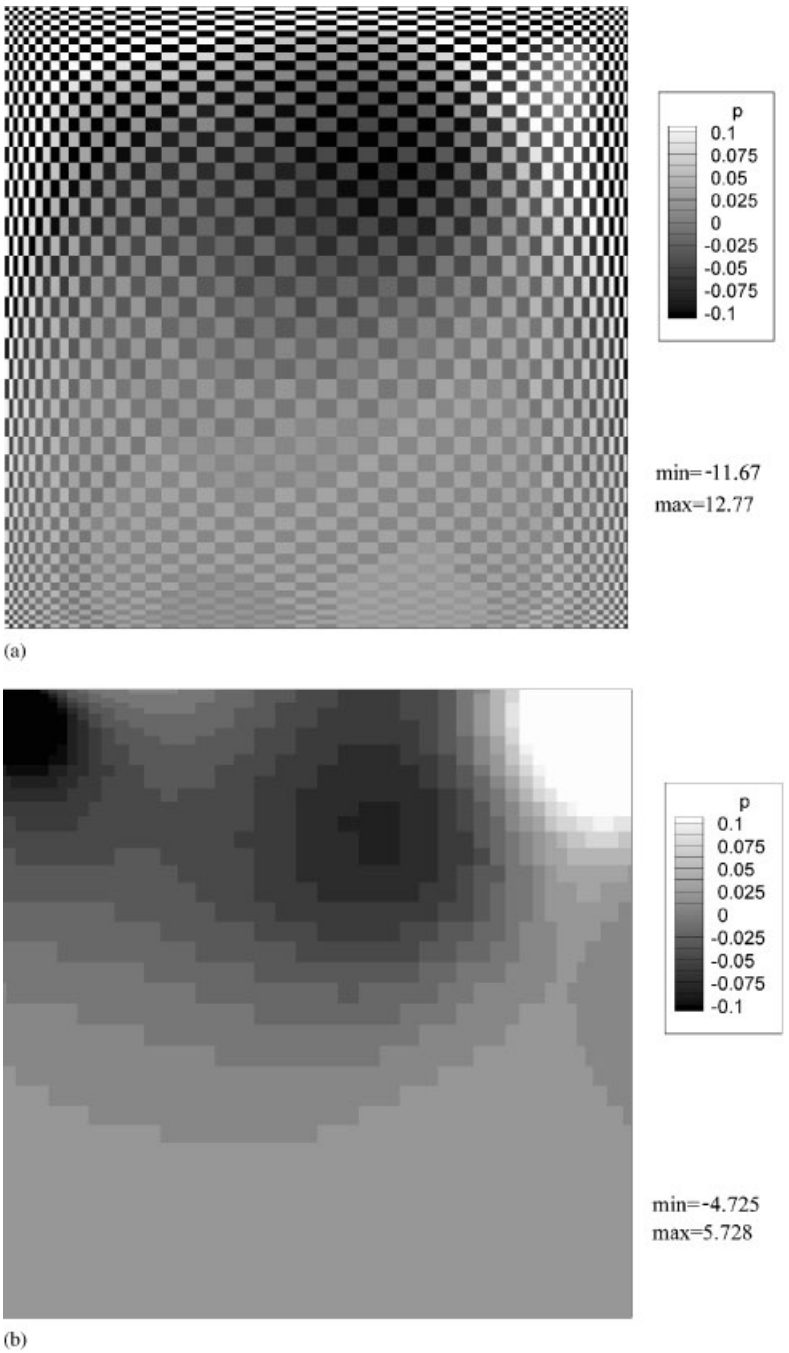

Figure 2. Element pressures: (a) $\beta = 0.01$, $\lambda = 1 \times 10^{-6}$; (b) $\beta = 1$, $\lambda = 1 \times 10^{-6}$ and (c) $\beta = 100$, $\lambda = 1 \times 10^{-6}$.

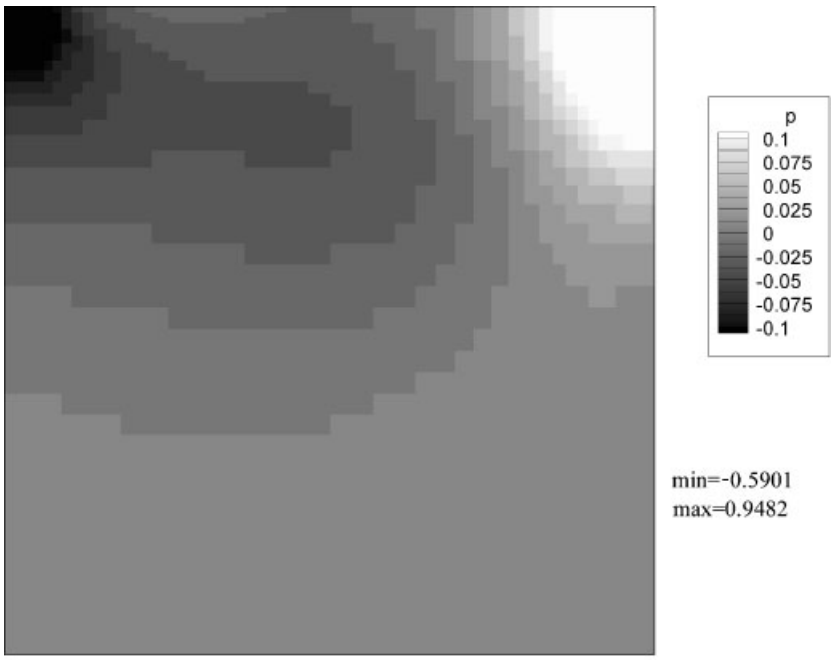

(c)

Figure 2. *Continued.*

4.1.2. λ-sensitivity. The time integration is advanced up to 20 *time units* (20 000 time steps) with various values of λ ranging from 10^{-15} to 1, starting with the same initial condition of zero internal velocity and zero pressure. Table III shows the global pressure integral, $\int_S p^h \, \mathrm{d}S$, the four local element pressures and a nodal velocity at the cavity centre, obtained finally. These numerical tests suggest that the global pressure integral approaches zero and the pressure solutions are hardly dependent on the parameter λ, as λ increases. It is also seen that the relative pressures and the velocity are hardly dependent on λ over the whole range tested here. This feature is consistent with Equation (16), which implies that the element-level velocity divergence is independent of λ.

Although the insensitivity of the solution to the parameter λ has been numerically shown with the above test, one cannot set the parameter λ at zero. If $\lambda = 0$, the matrix becomes singular due to the hydrostatic pressure mode and the PCG pressure solution can be extreme in magnitude (positive or negative) due to the arbitrariness of the additive constant. The extreme value of pressure could induce truncation errors and trigger numerical instability of a time integration. This is likely to occur especially when the PCG iteration step happens to be too large (or when the PCG convergence criterion is set too severely), as shown in the following section.

4.2. Three-dimensional driven cavity flow

The PCG convergence property is examined with the mixed method, the GPJ method and the proposed HPMS/GPJ method for both leaky and non-leaky 3-D driven cavity flow problems

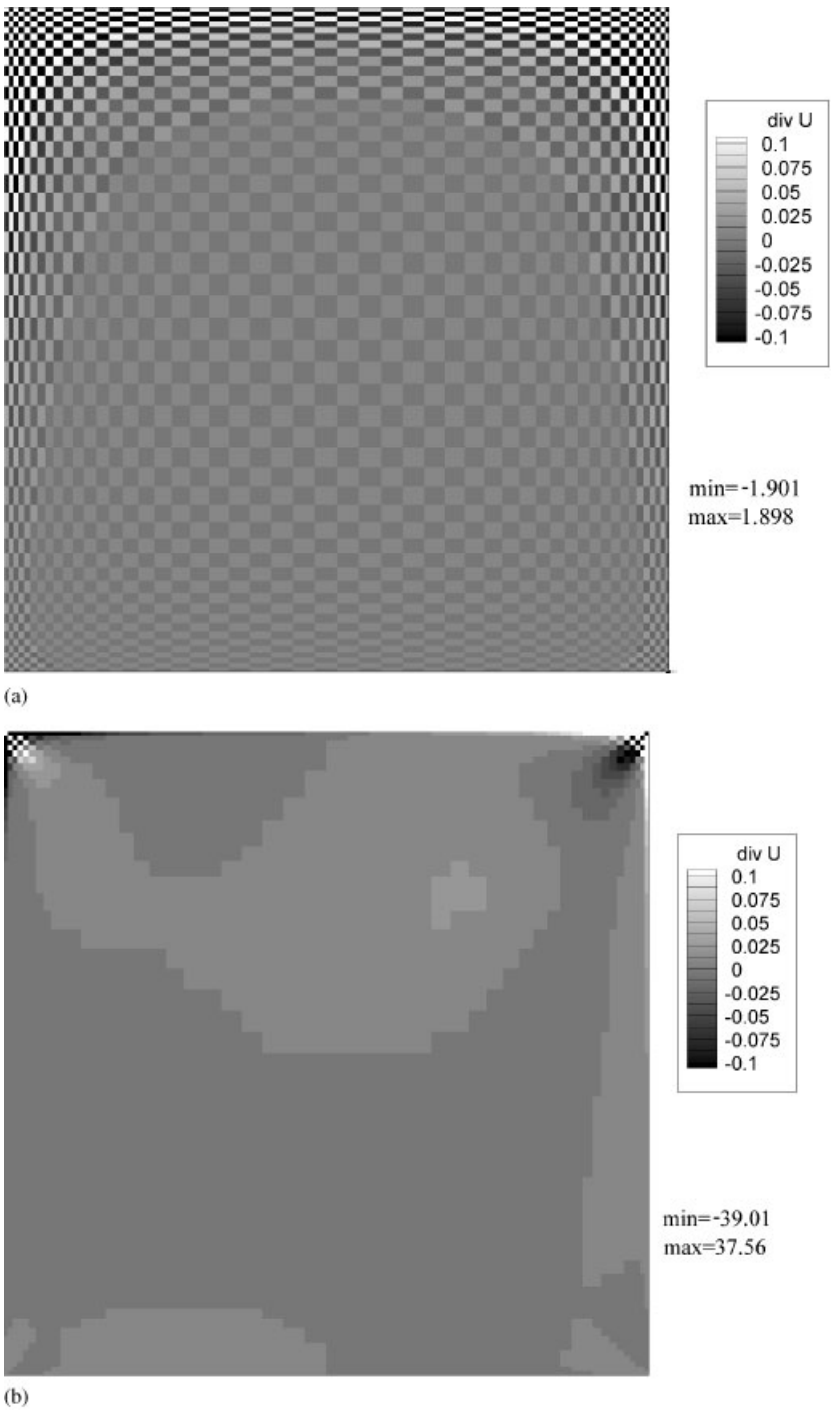

Figure 3. Element-level divergence of velocity: (a) $\beta = 0.01$, $\lambda = 1 \times 10^{-6}$; (b) $\beta = 1$, $\lambda = 1 \times 10^{-6}$ and (c) $\beta = 100$, $\lambda = 1 \times 10^{-6}$.

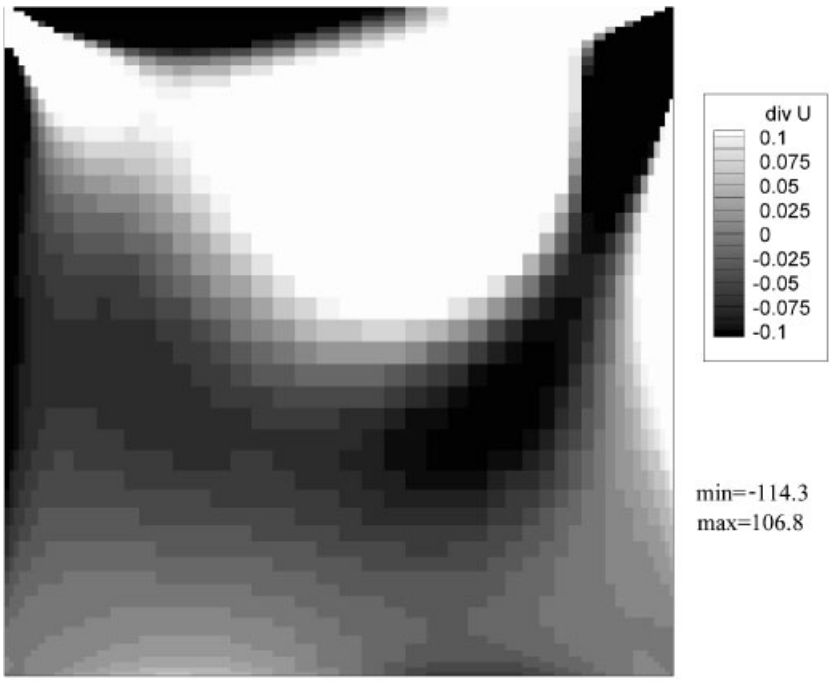

(c)

Figure 3. *Continued.*

at $Re = 100$ using $40 \times 40 \times 40$ Q1/P0 finite elements. Besides, the accuracy of the present method is also examined by solving the non-leaky cavity flow at $Re = 100$, 400 and 1000 for comparison with the previous reference results [10].

4.2.1. Leaky driven cavity flow. The upper lid on $z = 1$ including the four edges is driven towards positive y direction at unit velocity, while the other five walls are assumed as non-slip boundaries. The fluid can flow in and out through the most upper elements across the up- and down-stream cavity edges. The computations are started from the initial condition of zero internal velocity and zero pressure, and the convergence behaviours of the PCG solution for the pressure Poisson equation at the first corrector phase in the first time step are compared among the following methods:

(i) the mixed method ($\beta = \lambda = 0$),
(ii) the mixed method ($\beta = \lambda = 0$) with pressure pegging at one element,
(iii) the GPJ method ($\beta = 1, \lambda = 0$),
(iv) the GPJ method ($\beta = 1, \lambda = 0$) with pressure pegging at one element and
(v) the present HPMS/GPJ method ($\beta = 1, \lambda = 10^{-3}$).

The pressure pegging (PP) technique has been often and commonly used to rule out matrix singularity due to the hydrostatic pressure mode by imposing the Dirichlet condition on one

Table III. Effect of parameter λ on solutions at $t = 20$.

β	λ	$\int_S p^h \, dS$	Element pressure ($\times 10^{-2}$) p_{SW}	p_{SE}	p_{NW}	p_{NE}	u-velo.* / v-velo.*
	1×10^{-15}	-6.06×10^{-3}	-2.226	-2.264	-3.013	-3.104	-0.2088
			[0.878]	[0.840]	[0.091]	[—]	0.0561
1	1×10^{-9}	-5.74×10^{-3}	-2.194	-2.232	-2.981	-3.072	-0.2088
			[0.878]	[0.840]	[0.091]	[—]	0.0561
	1×10^{-3}	-3.84×10^{-11}	-1.620	-1.658	-2.408	-2.498	-0.2088
			[0.878]	[0.840]	[0.090]	[—]	0.0561
	1	2.47×10^{-16}	-1.620	-1.658	-2.408	-2.498	-0.2088
			[0.878]	[0.840]	[0.090]	[—]	0.0561

* Velocity solutions at the cavity centre node.
p_{SW}, p_{SE}, p_{NW} and p_{NE}: pressures of four neighbouring elements sharing the cavity centre node (pressures at the lower-left, lower-right, upper-left and upper-right of the node, respectively).
[ ]: pressure relative to p_{NE}.

element pressure (e.g. Reference [3]). In the computations with the methods (ii) and (iv), zero element pressure is imposed at the one of the bottom corner elements at the co-ordinates origin.

Figure 4 shows the distance norms of the residual vector of the Poisson equation up to 1500 PCG iterations unless the residual norm drops below 10^{-25}. It is seen that the convergences of the mixed methods with/without the PP are very slow. Even if the PCG iterations are continued up to 30 000 steps in the mixed methods, the residual norm has never been smaller than about 10^{-15}, moving up and down rather cyclically in the range from 10^{-3} to 10^{-15}. This is due to the matrix singularity associated with the spurious pressure mode (and also the hydrostatic pressure mode if the PP is not used), which is (are) more likely to appear as the PCG iteration number increases.

Although the convergences of the GPJ method and the HPMS/GPJ method are almost identical up to about 150 PCG iterations, the convergence property of the GPJ method without PP becomes anomalous after about 350 PCG iterations because of the hydrostatic singularity of the matrix. One practical strategy in the GPJ method without PP is to terminate the CG iteration before the anomalousness is brought about. However, it could be difficult to define the termination criteria for completely new problems in practical applications with complex geometries, because the CG convergence behaviours can be much more unpredictable for such problems. The anomalousness can be avoided by the PP in the GPJ method as seen in the figure, though selection of the element to be pegged at may require expertise in general, especially for a fully oscillatory flow.

On the other hand, the proposed HPMS/GPJ method (of course, *without* the PP trick) exhibits the fastest and steadiest convergence of the PCG iteration among the methods tested here.

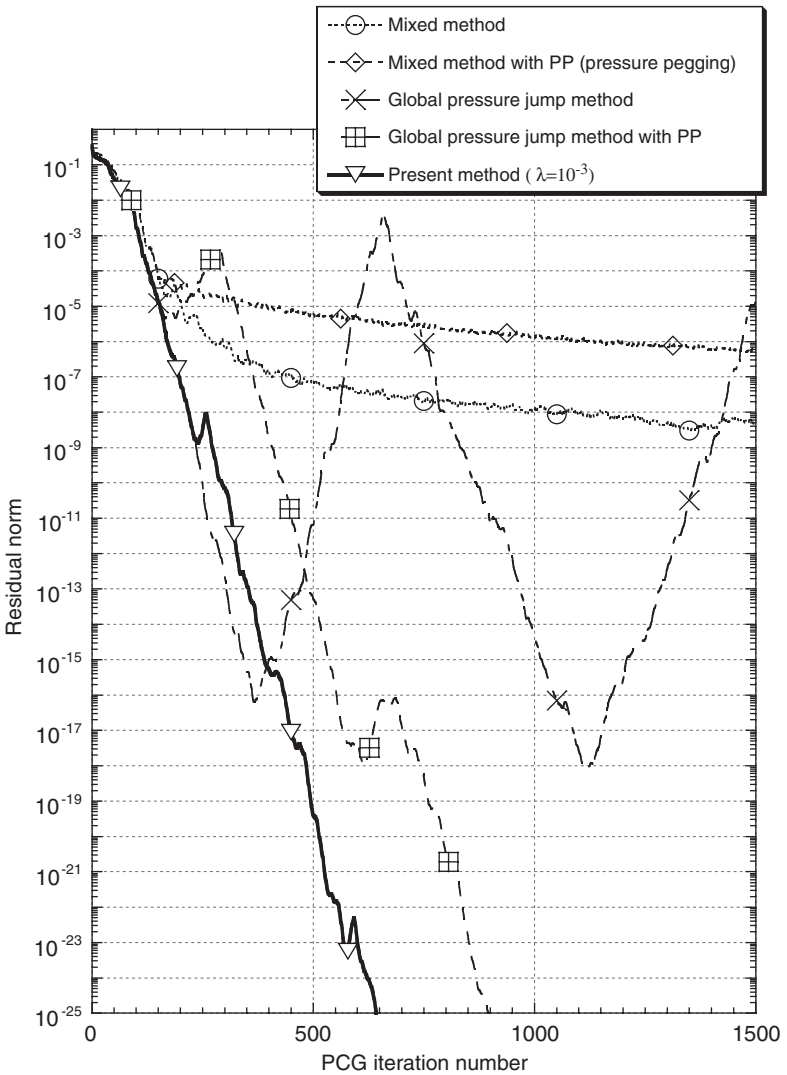

Figure 4. Convergence behaviour of PCG iteration for leaky cavity flow.

4.2.2. Non-leaky driven cavity flow. In the non-leaky cavity flow problem, the cavity is perfectly waterproof by imposing zero-velocity BC on all the edges as well as all the walls other than the upper driven wall. The convergence behaviours of the PCG solution for the pressure Poisson equation are similarly examined with the methods (i)–(v). Figure 5 shows the distance norms of the residual vector of the Poisson equation encountered first in the time integration starting from zero internal velocity and zero pressure. It is seen the norms in the mixed method with/without the PP are gradually increasing because of the ill-posed feature of this problem. The convergences in the other methods are very similar to those in the case

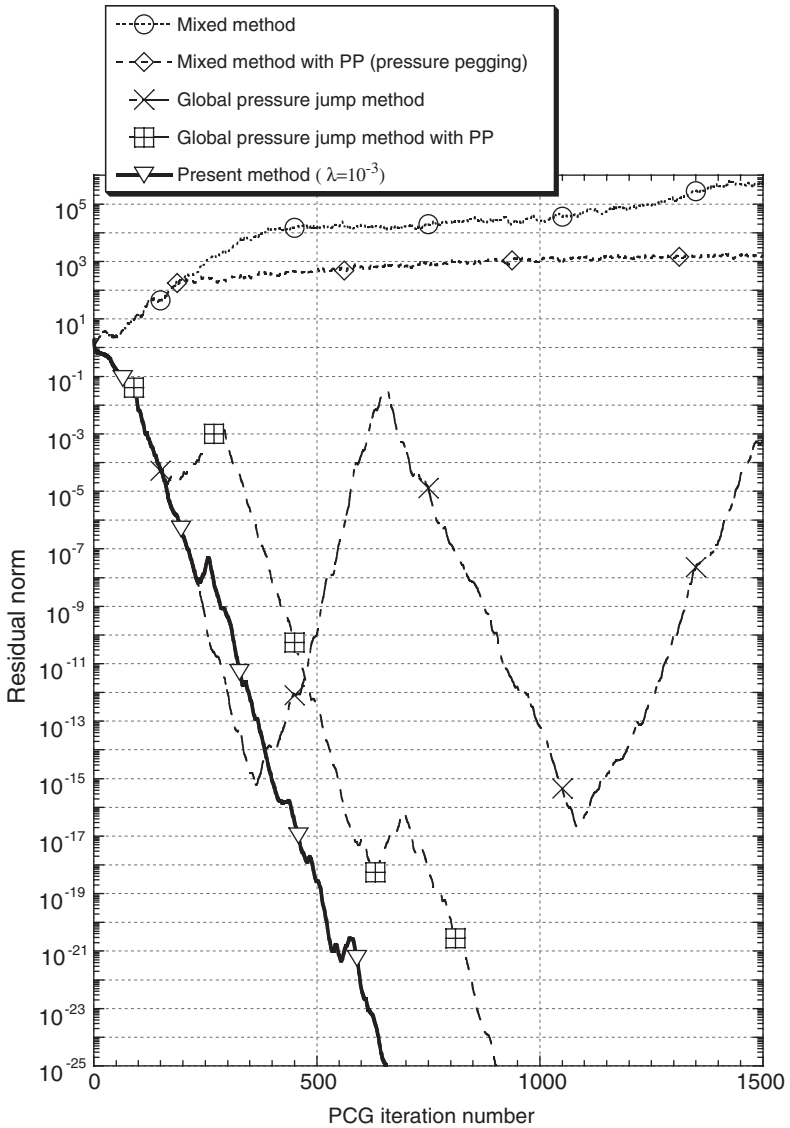

Figure 5. Convergence behaviour of PCG iteration for non-leaky cavity flow.

of the leaky cavity flow. The present method exhibits the best PCG convergence among them with almost constant convergence rate over the whole iteration step.

The non-leaky 3-D driven cavity flows at $Re = 100$, 400 and 1000 are solved by the HPMS/GPJ method ($\beta = 1, \lambda = 10^{-3}$) until the quasi-steady state is reached. That is, time integrations are performed 10 *time units* for $Re = 100$ starting with zero initial conditions, and the quasi-steady results of $Re = 400$ and 1000 are obtained at 20 and 30 *time units*,

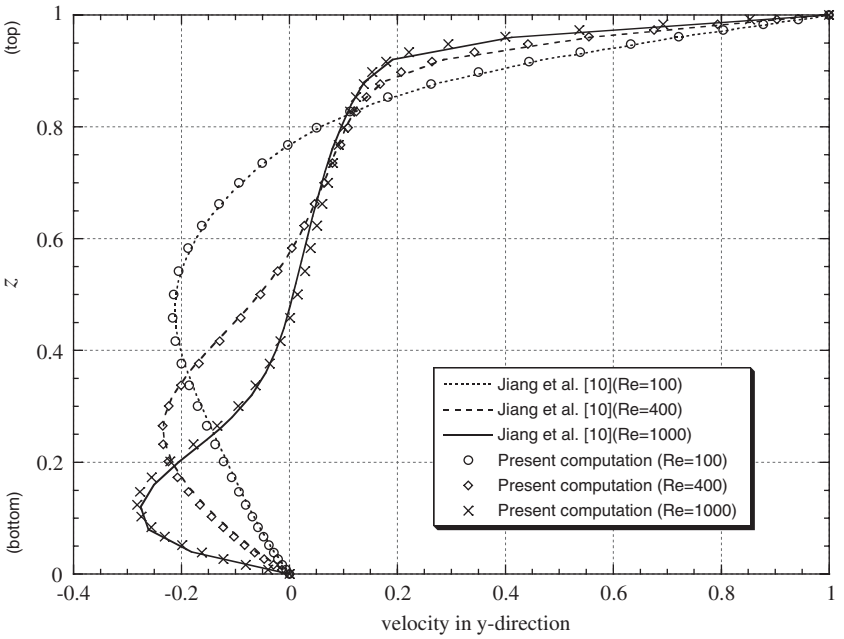

Figure 6. Velocity profile along the cavity centreline.

respectively, reducing the kinematic viscosity in a step-by-step manner. The results are compared with the literature data [10] where the least-squares FEM for the steady NS (velocity–pressure–vorticity) equations is used to solve the 3-D driven cavity flow with PP technique on $50 \times 50 \times 52$ equal-order trilinear elements (It is not stated in Reference [10] whether the BC is non-leaky or leaky, although the two thin element layers is placed near the driven lid to resolve the corner singularity). Figure 6 shows the velocity profiles (velocity component in the driving direction) along the centreline connecting the upper driven lid and the bottom wall. Despite the comparatively coarse mesh division of the present computation, the velocity profiles agree with those of Jiang *et al.* [10] very well. Figures 7(a) and 7(b) show the tomography of velocity vectors projected on the cut planes of $x = 0.5$ and $y = 0.5$, respectively. The velocity field seems reasonable as a whole, although weak spatial oscillations or wiggles of the velocity vectors are found near the upper cavity corners in Figure 7(a). The Taylor-Görtler-like vortices are observed near the bottom wall in Figure 7(b), which are quite similar to those depicted in the literature (Figure 6(a) in Reference [10]). Figures 8(a) and 8(b) show the raw element pressures on the cavity surface displayed in the full range from -0.7753 (the minimum pressure) to 1.532 (the maximum), and in a narrow range from -0.1 to 0.1, respectively. The overall pressure distribution seems reasonable, although some spurious pressure modes of minor amplitudes are found to concur with the velocity wiggles. On the other hand, the integral of the kinematic pressure over the whole domain, $\int_\Omega p^h \, d\Omega$, is close to zero, i.e. order of 10^{-8} to 10^{-9}, suggesting there is no hydrostatic pressure mode as expected in the present HPMS/GPJ formulation.

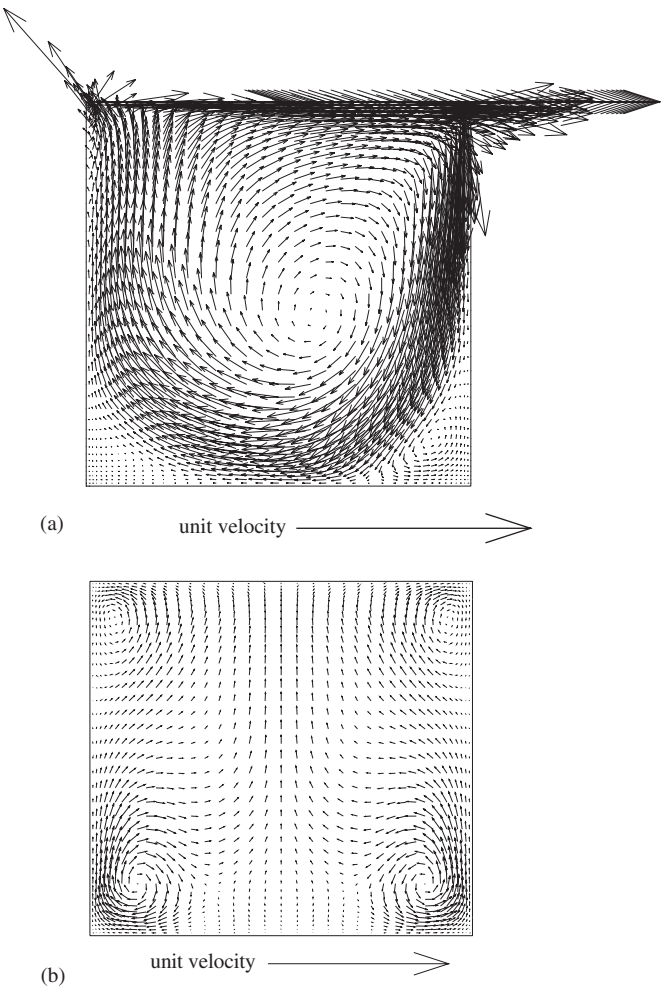

Figure 7. Tomography of velocity vectors cut by and projected on (a) $x = 0.5$ and (b) $y = 0.5$.

5. CONCLUSION

The author has proposed a positive definite regularization of the incompressible Stokes equations where the hydrostatic pressure mode appearing in confined flows can be eliminated with the newly introduced square-type linear form. The new regularization method, termed the HPMS/GPJ formulation here, has been implemented with Q1/P0 finite element approximation for the incompressible NS equations, employing the predictor/multi-corrector scheme as the time integrator. The computer code has been numerically tested for the NS solutions of 2-D and 3-D driven cavity flows. The results have revealed (1) insensitiveness of the solutions to the free parameter relating to the HPMS term, (2) the fast and steady PCG convergence

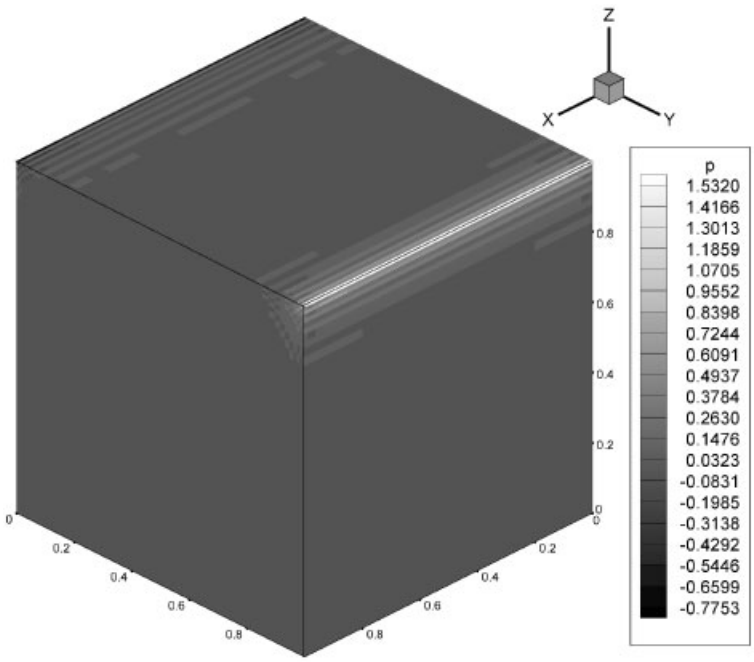

(a)

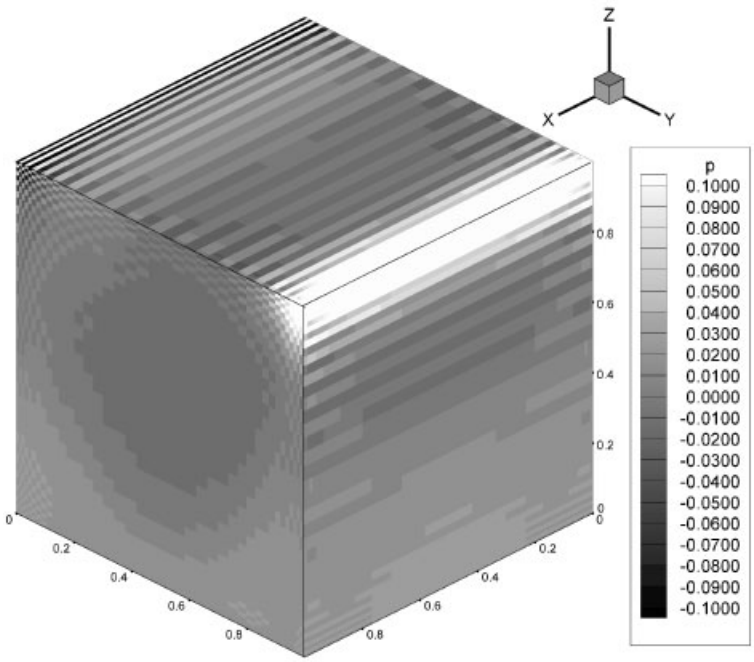

(b)

Figure 8. Element pressures on the cavity surface: (a) full range display and (b) narrow range display.

for the pressure Poisson solution and (3) the accuracy of nodal velocities and adequacy of element pressures.

It should be stressed that the HPMS method would be generally applicable for elimination of the hydrostatic pressure mode in any approximation methods with any types of elements (e.g. the local pressure jump method with the Silvester's macroelement or the mixed method with the elements satisfying the BB condition). The proposed HPMS regularization would free CFD analysts from the artificial pressure pegging for confined flows, giving bonus of fast and robust convergence of iterative solvers.

ACKNOWLEDGEMENTS

The author would like to express his sincere gratitude to Prof G. Yagawa, University of Tokyo, for his encouragement toward the present study. The enlightening comments given by the reviewers on some aspects on this work are also gratefully acknowledged.

REFERENCES

1. Hughes TJR, Franca LP. A new finite element formulation for computational fluid dynamics: VII The Stokes problem with various well-posed boundary conditions: Symmetric formulations that converge for all velocity/pressure spaces. *Computer Methods in Applied Mechanics and Engineering* 1987; **65**:85–96.
2. Silvester DJ, Kechkar N. Stabilised bilinear-constant velocity-pressure finite elements for the conjugate gradient solution of the Stokes problem. *Computer Methods in Applied Mechanics and Engineering* 1990; **79**:71–86.
3. Gresho PM, Sani RL. *Incompressible flow and the finite element method*, *volume 2*: *Isothermal laminar flow*. Wiley: Chichester, 1998.
4. Hughes TJR, Liu WK, Brooks A. Finite element analysis of incompressible viscous flows by penalty function formulation. *Journal of Computational Physics* 1979; **30**:1–60.
5. Sani RL, Gresho PM, Lee RL, Griffiths DF, Engelman M. The cause and cure (!) of the spurious pressures generated by certain FEM solutions of the incompressible Navier–Stokes equations: Part 2. *International Journal for Numerical Methods in Fluids* 1981; **1**:171–204.
6. Eguchi Y. Practical techniques for a three-dimensional FEM analysis of incompressible fluid flow contained with slip walls and a downstream tube bundle. *International Journal for Numerical Methods in Fluids* 2001; **37**:279–295.
7. Brooks AN, Hughes TJR. Streamline upwind/Petrov–Galerkin formulations for convection dominated flows with particular emphasis on the incompressible Navier–Stokes equations. *Computer Methods in Applied Mechanics and Engineering* 1982; **32**:199–259.
8. Eguchi Y. On streamline diffusion arising in Galerkin FEM with predictor/multi-corrector time integration. *International Journal for Numerical Methods in Fluids* 2002; **39**:1037–1052.
9. Ghia U, Ghia N, Shin CT. High-Re solutions for incompressible flow using the Navier-Stokes equations and a multi-grid method. *Journal of Computational Physics* 1982; **48**:387–411.
10. Jiang B-N, Lin TL, Povinelli LA. Large-scale computation of incompressible viscous flow by least-squares finite element method. *Computer Methods in Applied Mechanics and Engineering* 1994; **114**:213–231.

